Versatile biomimetic dendrimer templates used in the formation of TiO_2 and GeO_2†

Sarah L. Sewell,[a] Ryan D. Rutledge[b] and David W. Wright*[b]

Received 19th February 2008, Accepted 2nd May 2008
First published as an Advance Article on the web 13th June 2008
DOI: 10.1039/b802842g

Biomimetic synthesis is emerging as an advantageous alternative to the harsh synthetic conditions traditionally used in metal oxide syntheses techniques. Silaffins, proteins from the *C. fusiformis* diatom, form silica in an aqueous environment under benign conditions. Amine terminated PAMAM and PPI dendrimers are effective mimics of silaffins and other silica precipitating polyamines. We have expanded the scope of dendrimer mediated metal oxide formation to include titanium dioxide, a photocatalyst, and germanium dioxide, a blue photoluminescent material. The nanoparticles were characterized using scanning electron microscopy (SEM), Fourier transform infrared spectroscopy (IR), and X-ray diffraction patterns (XRD). A variable temperature XRD analysis of TiO_2 nanoparticles was conducted to study the transition from anatase to rutile. TiO_2 nanoparticles synthesized in phosphate buffer showed a 200 °C decrease in the anatase to rutile transition temperature relative to TiO_2 templated in water. XRD analysis of GeO_2 nanoparticles in either water or phosphate buffer reveal crystalline α-phase germanium oxide. To our knowledge, this is the first report of the synthesis of crystalline GeO_2 under ambient conditions.

Introduction

Many techniques used for metal oxide synthesis require harsh environments such as high temperatures, extreme pH, and caustic conditions.[1,2] Conversely, nature forms a myriad of metal oxides under ambient, aqueous conditions.[3] For example, the oriental hornet, *Vespa orientalis*, incorporates crystalline iron titanium oxide into the cell walls of its nests as a gravity reference point.[4,5] Magnetotactic bacteria crystallize iron oxide for alignment with the earth's magnetic field.[6] Furthermore, ferritin, a 450 kD storage protein found in most mammals, stores iron by mineralizing iron oxohydroxide nanoparticles.[7] By emulating the chemistry of these natural mineralization pathways, abiological materials can be formed. For example, the electrostatic environment of ferritin has been used to mineralize oxohydroxides of cobalt, manganese, and nickel.[8–10] The biomineralization pathways of sponges and diatoms also serve as relevant examples for the formation of diverse metal oxides. Morse and coworkers have extensively studied the silica producing proteins, silicateins, derived from sponge spicules.[11] Through point mutation studies, histidine and serine were identified as the catalytic components in the active site of the protein, leading to the hydrolysis and condensation of tetraethoxysilane to form silica.[12] Silicatein filaments have also formed titanium dioxide and gallium oxide from non-natural substrates, demonstrating that the chemistry of the silicatein filament can accommodate a variety of substrates.[13,14]

Another biosilification mechanism that has been expanded to form non-natural metal oxides is the mineralization pathway of the peptides derived from the diatom *Cylindrotheca fusiformis.* Silaffins, isolated from *C. fusiformis*, have been shown to form silica at pH 5.5. Structural analysis of one such silaffin, Nat-Sil1A, revealed that serine residues were phosphorylated and the lysine were post-translationally modified forming ε-*N*-dimethyl-lysine, ε-*N*-trimethyl-δ-hydroxylysine, and long chain polyamines, derivatives of polypropyleneimine.[15,16] In addition to silaffins, a biomimetic analogue derived from a repeat unit of the Natsil gene, the R5 peptide (SSKKSGSYSGSKGSKRRIL), precipitates silica from monosilicic acid.[17,18] Mutation studies of the R5 peptide have shown that the RRIL motif is critical for silica formation, as it causes the peptide to self-assemble, providing a locally high amine concentration, and promoting the subsequent condensation of monosilicic acid.[19] The biosilification pathway of the R5 peptide

[a]*Department of Biomedical Engineering, Vanderbilt Univeristy, Station B Box 351620, Nashville, TN, 37235, USA*
[b]*Department of Chemistry, Vanderbilt University, Station B 351822, Nashville, TN, 37235, USA. E-mail: david.wright@vanderbilt.edu; Fax: +1 615 343 1234; Tel: +1 615 322 2636*

† Electronic supplementary information (ESI) available: TiO_2 production as a function of G0 PAMAM primary amine concentration and of pH, GeO_2 production as a function of pH, SEM micrographs of TiO_2 nanoparticles precipitated in phosphate buffer and in water, IR spectra of TiO_2 precipitated in phosphate buffer and in water, variable temperature X-ray diffraction spectra of TiO_2 precipitated in phosphate buffer and in water, SEM micrographs of GeO_2 nanoparticles precipitated in phosphate buffer and in water, IR spectra of GeO_2 precipitated in phosphate buffer and in water, variable temperature X-ray diffraction spectra of TiO_2 precipitated in phosphate buffer and in water, variable temperature X-ray diffraction spectra of G4 PAMAM templated GeO_2 in water and in phosphate buffer, XRD of GeO_2 with TIPG used as the precursor, PLL templated GeO_2 XRDs, GeO_2 production as a function of primary amine concentration using TMOG, TIPG, and TEOG as the precursor, IR spectra of GeO_2 particles when TMOG and TIPG are used as the precursor, SEM images of GeO_2 particles when TMOG and TIPG are used as the precursor, light scattering profile of G4 dendrimer templated TiO_2 reaction and G4 dendrimer templated GeO_2 reaction in water. See DOI: 10.1039/b802842g

as well as recombinant silaffins have been expanded to include substrates such as titanium bis(ammonium lactato) dihydroxide (TBALDH, $[CH_3CH(O^-)CO_2NH_4]_2Ti(OH)_2$), resulting in the formation of TiO_2.[20,21]

Moreover, diatoms also contain long chain polyamines such as N-methylated poly(propylene imines) attached to putrescine cores that are capable of precipitating silica.[16] Patwardhan and coworkers have investigated the ability of poly-L-lysine (PLL), as well as a variety of other cationic polymers such as poly-L-histidine, poly(allylamine) hydrochloride, poly-L-arginine, and polyethyleneimine to form silica from monosilicic acid *in vitro*.[22–27] The positively charged polymer template assembles the silicic acid species through electrostatic interactions and hydrogen bonding. This interaction results in the aggregation and subsequent condensation to form silica.[28–30] In addition to silica, metal oxides such as germanium oxide and titanium oxide have been formed when PLL is used as the template, demonstrating that the mechanism of PLL-mediated metal oxide formation can be expanded to accommodate non-natural substrates.[20,31]

Increasingly dendrimers are being used as monomolecular templates for nanoparticle formation and stabilization in a variety of systems.[32–36] Using carboxylated phosphorus dendrimers as templates, sol–gel techniques have been used to form porous, amorphous networks of TiO_2 and GeO_2.[32] Upon thermal treatment, the dendrimer template was removed. Carboxylated PAMAM dendrimers (G4.5) have been used in concert with ammonium hydroxide to form agglomerated powders of amorphous zirconium oxide, caesium oxide, and yttrium oxide.[33] Upon heating, nanocrystalline metal oxide powders were obtained. Additionally, dendrimers have been used as stabilizing templates to increase the photocatalytic activity of TiO_2 nanoparticles.[35,36] In contrast to these highly processed sol–gel techniques, amine terminated dendrimers mimic the chemistry of diatoms to form silica at room temperature in an aqueous environment.[34] Polyamidoamine (PAMAM) dendrimers are composed of ethylenediamine units with surface amine groups, similar to the unmodified lysine in the R5 peptide, while polypropyleneimine (PPI) dendrimers consists of repeating polyeneimine units that are similar to the modified lysines in native silaffins and polyamines. The primary amine moieties of the dendrimer are thought to concentrate and drive the condensation of the monosilicic acid, forming silica nanoparticles.[34,37]

Biomimetic approaches are being used to synthesize a menagerie of materials not found in nature.[9,10,13,14,31,38–40] Titanium dioxide (TiO_2) is a photocatalytic material used in sunscreen, white paint pigment and has the potential to be used in environmental applications such as water purification, wastewater treatment, and air purification.[41,42] Germanium dioxide (GeO_2) is a blue photoluminescent material with a higher refractive index than silica that is being investigated as a material for optical wave guides in integrated optical systems.[43,44] At room temperature under ambient conditions, PAMAM (G0, G2, G4 and G6) and PPI (G4 and G5) dendrimers rapidly form TiO_2 and GeO_2 from the precursors TBALDH and tetramethoxygermanium ($Ge[OCH_3]_4$, TMOG), tetraethoxygermanium ($Ge[OCH_2CH_3]_4$, TEOG), or tetraisopropoxygermanium ($Ge[OCH(CH_3)_2]_4$, TIPG) germanium alkoxides, respectively. The nanoparticles were characterized using scanning electron microscopy (SEM), Fourier transform infrared spectroscopy (IR), X-ray diffraction patterns (XRD), and photoluminescent spectroscopy.

Experimental

Chemicals

PAMAM and PPI dendrimers (all generations) were purchased from Sigma Aldrich. The purity of all dendrimers is greater than 90% and the polydispersity ranges from 1.05–1.10, as reported by Sigma Aldrich. All metal oxide precursors (titanium(IV) bis(ammonium lactato) dihydroxide (TBALDH), tetramethoxygermanium (TMOG), tetraethoxygermanium (TEOG), or tetraisopropoxygermanium (TIPG) were purchased from Sigma Aldrich.

TiO_2 precipitation assay

Titanium(IV) bis(ammonium lactato) dihydroxide (40 μL, 1 M) was added to dendrimer solutions ranging from 2.5 to 100 mM primary amine concentration diluted in either 200 μL phosphate buffer (100 mM, pH 7.5) or water, resulting in final metal to primary amine ratios ranging from 80 : 1 to 2 : 1. The reactions were shaken for 5 min, centrifuged for 5 min at 10000 rpm, and washed three times with deionized water.

GeO_2 precipitation assay

Tetramethoxygermanium (TMOG), tetraethoxygermanium (TEOG), or tetraisopropoxygermanium (TIPG) (5 μL, neat) were added to dendrimer solutions ranging from 2.5 to 100 mM primary amine concentration diluted in either 200 μL phosphate buffer (100 mM, pH 7.5) or water, giving metal to primary amine ratios ranging from 70 : 1 to 1 : 1. When poly-L-lysine (PLL) was used as the biomimetic template, TMOG, TEOG, or TIPG were introduced into a solution of 4 mg mL^{-1} PLL·HBr (average molecular weight: 55000 g mol^{-1}) in phosphate buffer (100 mM, pH 7.5). The reactions were shaken for 5 min, centrifuged for 5 min at 10000 rpm and washed three times with deionized water. **NOTE:** It is absolutely imperative to use fresh precursor for each reaction.

Titanium quantitation

The 5-chlorosalicylic acid assay was used to quantitate TiO_2 production.[45] TiO_2 was dissolved in 1 mL of concentrated sulfuric acid and incubated at 95 °C for 2 h. 5-Chlorosalicylic acid (2.5 mL of 2.5% in ethanol), sodium perchlorate (2.5 mL, 1 M), ethanol (7.5 mL), and deionized water (10 mL) were added to the dissolved titanium solution. The solution was adjusted to pH 4 using concentrated NH_4OH and diluted to 50 mL using deionized water. The colorimetric product was monitored at 355 nm using an Agilent 8453 UV-Vis spectrophotometer and quantitated using a standard curve.

Germanium quantitation

The β-silicamolybdate assay described by Iler was modified to quantitate germanium oxide precipitation.[40,46] Ammonium paramolybdate $(NH_4)_6Mo_7O_{24}{\cdot}4H_2O$ (4.0 g) was dissolved in

300 mL of deionized water. Concentrated hydrochloric acid (12 mL) was added to the ammonium paramolybdate solution and diluted to 500 mL. Germanium dioxide was dissolved in 1 mL of 0.5 M NaOH at 95 °C for 30 min. The dendrimers interfered with the assay so they were removed by Centricon filtration (Amicon Centricon filtration devices, Millipore, Inc). Due to available molecular weight cutoff filters, only templates with molecular weights higher than 3000 were assayed. To 0.5 mL of the filtered solution, 5 mL of the ammonium molybdate solution was added and allowed to react for 15 min. The colorimetric product was monitored at 410 nm using an Agilent 8453 UV-Vis spectrophotometer and quantitated using a standard curve.

Reseeding experiments

GeO_2 or TiO_2 precipitation assays were conducted as stated above using water as the solvent. The nanoparticles were collected by centrifugation and extensively washed with water to remove any unreacted dendrimer. The nanoparticles were suspended in 200 μL of water and either 5 μL of neat tetraethoxygermanium or 40 μL of TBALDH was added to the solution. The reactions were shaken for 5 min, washed 3 times with water, and quantitated using the respective assays.

X-Ray diffraction

Powder X-ray diffraction (XRD) scans were obtained on a Scintag X_1 θ/θ automated powder diffractometer with a Cu target, a Peltier-cooled solid state detector, and a zero background Si(510) sample support. For titanium dioxide, the samples were scanned from 20 to 60 2Θ with a step size of 0.02 and a preset time of 25 s. Germanium oxide samples were scanned from 18 to 50 2Θ with a step size of 0.03 and a scan time of 10 s. For high temperature scans, the samples (15 mg) were heated to the appropriate temperature for 2 h in a sealed quartz tube in a 79300 Thermolyne tube furnace under nitrogen. All peaks were identified according to JCPDS.

Scanning electron microscopy

The nanoparticles were examined using a Hitachi S4200 scanning electron microscope (SEM) operating at variable voltages. The samples were suspended in ethanol and added dropwise to an aluminium SEM puck (Ted Pella Inc.). After evaporation of the solvent, the samples were sputter coated with a thin layer of gold (Pelco Model 3 Sputtering Instrument) to avoid charging.

Infrared spectroscopy

TiO_2 and GeO_2 were prepared in the precipitation assays stated above. After the final wash, the samples were dried under vacuum and pressed into KBr pellets. The samples were analyzed on a Mattson Genesis Series FTIR.

Photoluminescence spectroscopy

GeO_2 or TiO_2 were prepared in the precipitation assays stated above. After the final wash, the samples were dried under vacuum. The samples were analyzed using a Varian Cary Eclipse fluorescence spectrophotometer. GeO_2 nanoparticles were excited at 325 nm and the photoluminescence spectrum was collected from 350 to 600 nm with data intervals of 0.5 nm and an averaging time of 1.0 s. TiO_2 nanoparticles were excited at 280 nm and the photoluminescence spectrum was collected from 300 to 600 nm with data intervals of 0.5 nm and an averaging time of 1.0 s.

Selected area diffraction patterns

GeO_2 nanoparticles were analyzed on a Philips CM 20T transmission electron microscope (TEM) operating at 200 kV. Samples were prepared by pipetting the nanoparticle solution on a 3 mm diameter nickel grid covered with carbon film as a substrate (SPI supplies) and allowed to evaporate.

Light scattering experiments

Light scattering data was obtained using a Agilent 8453 UV-Vis Spectrophotometer. Typical TiO_2 and GeO_2 precipitations, as described above, were performed in a cuvette while simultaneously monitoring the absorbance at 480 nm throughout the duration of the reaction.

Results and discussion

A series of dendrimers (PAMAM G0–G6 and PPI G5–G4) were assayed for their ability to rapidly precipitate either TiO_2 or GeO_2 nanospheres from a solution of TBALDH or the appropriate germanium alkoxide precursor (Table 1). All templates assayed were active and yielded metal oxide nanoparticles. When the precursors were introduced into control solutions (containing either G4.5 PAMAM dendrimers or G4-OH dendrimers) and solutions lacking dendrimers, no particle formation was observed. This indicates that the primary amine moieties drive the formation of the metal oxide species. In the case of TiO_2, the 5-chlorosalicylic acid assay was used to determine the amount of titanium produced.[45] As the generation of dendrimer increased, the specific activity of the template increased accordingly (Table 1). A linear correlation between primary amine concentration and metal oxide production activity was observed for both classes of dendrimer under non-limiting conditions (Fig. 1 and ESI†). In the case of TiO_2, there is a linear increase of oxide formed between 0 and 40 mM dendrimer primary amine concentration that subsequently plateaus near 20000 nanomoles of TiO_2. Unlike the R5 peptide, the amount of TiO_2 formed does not vary as a function of pH (ESI†).[20]

Similar to TiO_2 and silica production, the specific activity of GeO_2 increases with increasing dendrimer generation and varies as a function of dendrimer primary amine concentration (Table 1 and Fig. 2).[34] The amount of GeO_2 produced was quantified using a variation of the β-silicomolybdate assay described by Iler.[46] As the dendrimers interfered with the assay, they were separated from the solution using molecular weight filtration. As the germanium substrate becomes limiting at approximately 30 mM primary amine concentration, GeO_2 production plateaus at approximately 12000 nanomoles (Fig. 2A). PPI dendrimer displayed a similar activity profile (Fig. 2B). Similar to TiO_2

Table 1 Dendrimer activity

Dendrimer	Template size/Å	Number of primary amines	Metal oxide species[a]	Solvent[b]	Specific activity[c]	Size of nanoparticles/nm[d]
G0 PAMAM	15	4	TiO_2	Water	1.5 ± 0.2	60 ± 15
	15	4	TiO_2	Phosphate buffer (100 mM, pH 7.5)	6.9 ± 0.6	310 ± 80
	15	4	GeO_2	Water	ND	110 ± 40
	15	4	GeO_2	Phosphate buffer (100 mM, pH 7.5)	ND	480 ± 170
G2 PAMAM	29	16	TiO_2	Water	23.1 ± 1.5	60 ± 15
	29	16	TiO_2	Phosphate buffer (100 mM, pH 7.5)	20.8 ± 3.1	380 ± 250
	29	16	GeO_2	Water	ND	120 ± 35
	29	16	GeO_2	Phosphate buffer (100 mM, pH 7.5)	ND	470 ± 280
G4 PAMAM	45	64	TiO_2	Water	89.6 ± 10.4	60 ± 30
	45	64	TiO_2	Phosphate buffer (100 mM, pH 7.5)	100.6 ± 8.6	430 ± 150
	45	64	GeO_2	Water	24.2 ± 2.5	80 ± 60
	45	64	GeO_2	Phosphate buffer (100 mM, pH 7.5)	26.4 ± 4.1	350 ± 150
G6 PAMAM	67	256	TiO_2	Water	273.5 ± 38.9	50 ± 15
	67	256	TiO_2	Phosphate buffer (100 mM, pH 7.5)	253.45 ± 35.8	470 ± 90
	67	256	GeO_2	Water	91.3 ± 13.4	80 ± 20
	67	256	GeO2	Phosphate Buffer (100 mM, pH 7.5)	114.9 ± 13.9	460 ± 190
G4 PPI	23.2	32	TiO_2	Water	31.8 ± 1.9	50 ± 20
	23.2	32	TiO_2	Phosphate buffer (100 mM, pH 7.5)	34.9 ± 3.0	220 ± 70
	23.2	32	GeO_2	Water	28.6 ± 3.0	40 ± 20
	23.2	32	GeO_2	Phosphate buffer (100 mM, pH 7.5)	19.3 ± 3.3	290 ± 150
G5 PPI	27.8	64	TiO_2	Water	84.9 ± 13.5	40 ± 20
	27.8	64	TiO_2	Phosphate buffer (100 mM, pH 7.5)	104.4 ± 14.0	200 ± 90
	27.8	64	GeO_2	Water	66.6 ± 3.1	30 ± 10
	27.8	64	GeO2	Phosphate buffer (100 mM, pH 7.5)	44.3 ± 5.5	330 ± 160

[a] TEOG was used as the precursor for GeO_2 reactions. [b] The pH for reactions run in deionized water was 5.5. [c] Specific activity is reported as nanomoles metal oxide per min × nanomole dendrimer. [d] As determined using SEM.

activity, GeO_2 production did not vary as a function of pH (ESI†).

Representative SEM images of TiO_2 formed with G4 PAMAM dendrimers show round nanoparticles with a Gaussian size distribution centered at 60 nm (Fig. 3A). In water, the average sizes of PAMAM (G0, G2, G4, G6) templated TiO_2 ranged from 50 to 60 nm, while PPI templated TiO_2 average sizes were 50 and 40 nm for G4 and G5 PPI, respectively (Table 1 and ESI†). In water, the average sizes of GeO_2 nanoparticles produced from the PAMAM (G0, G2, G4, G6) templates ranged from 80 to 120 nm, while average PPI templated particle sizes were 40 nm for G4 PPI and 50 nm for G5 PPI (Fig. 3B). When phosphate ions were introduced, the sizes of the PAMAM and PPI templated TiO_2 and GeO_2 nanoparticles increased. A similar trend was seen with silica nanoparticle formation by Knecht and coworkers.[47] The presence of cations in solution is proposed to neutralize the charge of the ripening nanoparticle, allowing it to stay in solution longer, resulting in a larger particle. The average size of PAMAM (G0, G2, G4, and G6) dendrimer templated TiO_2 and GeO_2 nanoparticles formed in phosphate buffer ranged from 310 to 470 nm and 350 to 480 nm, respectively (Fig. 3C and D). Interestingly, nanoparticles formed using PPI dendrimers as a template in phosphate buffer were much smaller with average sizes of 200 nm (G5 PPI) and 220 nm (G4 PPI) for TiO_2 and 290 nm (G4 PPI) and 330 nm (G5 PPI) for GeO_2. A comparison between PAMAM and PPI dendrimers with the same number of amines reveals that the ratio of the template diameter is consistent with the ratio of metal oxide nanosphere diameters formed using these respective dendrimers (Table 1), suggesting that the metal oxide-encapsulated dendrimer is the aggregating unit of oxide growth.[34] The sizes of the TiO_2 and GeO_2 nanoparticles are consistent with dendrimer templated silica nanoparticles, as well as R5 templated silica and TiO_2 nanoparticles.[20,34,48]

TiO_2 nanoparticles from each generation synthesized in the presence of water or phosphate were analyzed using IR spectroscopy (ESI†). The Ti–O–Ti absorption band ranging from 500 to 600 cm^{-1} was observed in all TiO_2 samples.[32] In each PAMAM templated TiO_2 sample, amide I and II stretching frequencies at approximately 1650 and 1540 cm^{-1} were present, indicating the association of the template with the nanoparticles.[49] Similarly, the amine frequency was observed at approximately 1650 cm^{-1} in the IR spectra of PPI templated TiO_2 nanoparticles.[49] Additionally, when phosphate buffer was present, broad peaks ranging from 966 to 996 cm^{-1} were present due to the P–O vibration frequency also seen in a variety of metal oxides synthesized in the presence of phosphate.[20,50–53]

The IR analysis for GeO_2 nanoparticles synthesized in the presence of PAMAM and PPI showed the Ge-O-Ge stretching frequency ranging from 790 to 890 cm^{-1} (ESI†).[54–57] Additionally, the amide I and II stretching frequencies were present in the PAMAM templated nanoparticles. However, in the samples synthesized in the presence of phosphate buffer, the phosphate vibration frequency was not present. This indicates that there is no phosphate associated with the metal oxide species.[49]

The principle applications of metal oxides are related to their photoluminescent properties. For example, anatase TiO_2 is reportedly a better photocatalyst than rutile TiO_2 due to the oxygen vacancies in the metal oxide.[58] Anatase TiO_2 displays a photoluminescent band centered around 500 nm due to these

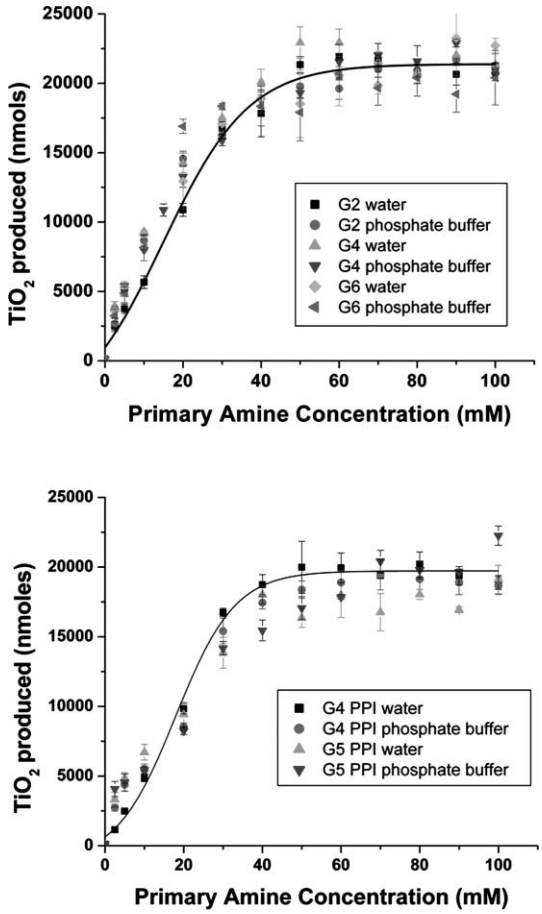

Fig. 1 Top: G2, G4, and G6 PAMAM templated TiO_2 production as a function of primary amine concentration in phosphate buffer (100 mM, pH 7.5) and water. Bottom: G4 and G5 PPI templated TiO_2 production as a function of primary amine concentration in phosphate buffer (100 mM, pH 7.5) and water. The maximum amount of TiO_2 produced in these samples corresponds to approximately 50% of initial metal conversion.

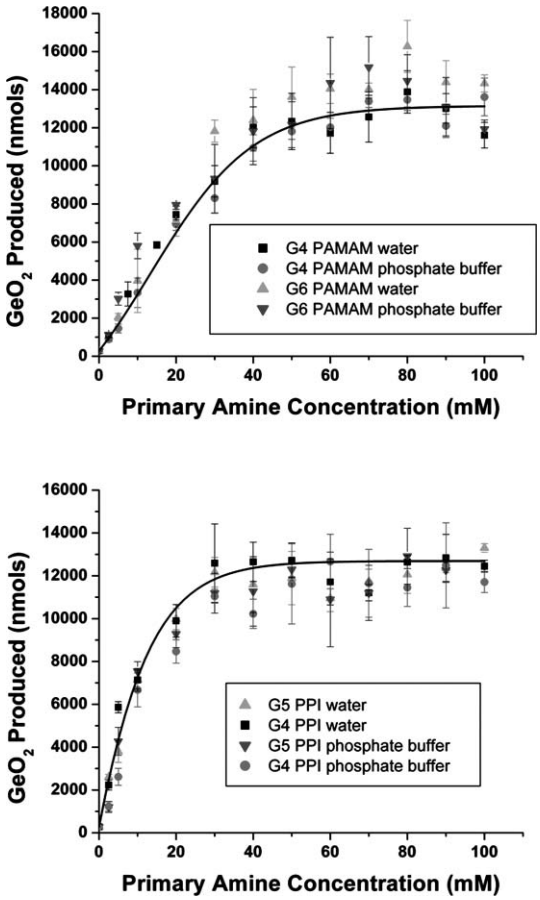

Fig. 2 Top: G4 and G6 PAMAM templated GeO_2 production as a function of primary amine concentration in phosphate buffer (100 mM, pH 7.5) and water using TEOG as the germanium alkoxide precursor. Bottom: G4 and G5 PPI templated GeO_2 production as a function of primary amine concentration in phosphate buffer (100 mM, pH 7.5) and water using TEOG as the germanium alkoxide precursor. The maximum amount of TiO2 produced in these samples corresponds to approximately 60% of initial metal conversion.

oxygen vacancies, while rutile does not.[58] The as synthesized TiO_2 dendrimer templated nanoparticles are isolated as an amorphous phase, and thus did not exhibit photoluminescent properties. In contrast, silicatein templated TiO_2, which was shown to consist of a mixture of amorphous and anatase crystalline phases, demonstrated an emission maximum at 480 nm when excited at 280 nm.[13] The photoluminescent properties of GeO_2 are being investigated for future applications in integrated optical devices.[43,44] GeO_2 templated nanocrystals revealed a photoluminescent emission at 420 nm (3.1 eV) when excited at 325 nm (Fig. 4). Reported photoluminescent spectra for GeO_2 varies widely depending on the excitation wavelength, the physical form of GeO_2 (*i.e.* wires, fibers, nanocrystals), and the amount of defects in the material.[57,59–66] The emission observed here is consistent with GeO_2 nanocrystals that had been previously synthesize from high temperatures that have been excited at 325 nm.[59–61]

The formation of amorphous TiO_2 at room temperature has been reported for a variety of amine-terminated molecules, including silicateins, the R5 peptide, and silaffin proteins.[13,20,21] It should be noted that despite the similar interactions involving terminal amines, at no point did the dendrimers produce as-synthesized particles that contained a degree of anatase or rutile crystallinity. These crystalline phases could only be achieved *via* thermal annealing. To examine the phase transition from anatase to rutile, variable temperature XRD analysis of TiO_2 synthesized in either water or phosphate buffer was conducted (Fig. 5A, B, and ESI†). The phase transition from distorted face centered cubic anatase to distorted hexagonal closest packed rutile is an intermediate topotactic phase transition with two Ti–O bonds breaking and reforming in the process.[67] Dendrimer templated TiO_2 synthesized from water was amorphous at room temperature. At 600 °C, TiO_2 annealed to crystalline anatase. At 700 °C, the rutile phase formed, with a complete transition from anatase to rutile present at 900 °C. This transition is consistent with the previously reported transition temperature of R5-templated TiO_2, but is slightly higher when compared to silicatein-templated TiO_2.[20,21] Similarly, TiO_2 nanoparticles condensed by PAMAM dendrimers in the presence of phosphate buffers were amorphous at room temperature. Upon heating to 600 °C, the crystalline anatase phase was observed. A

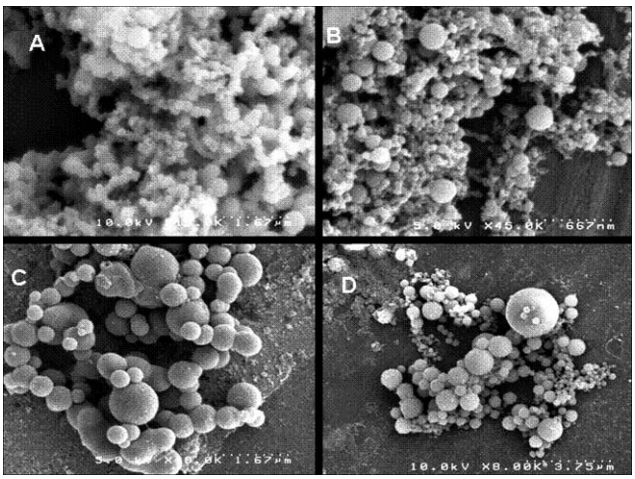

Fig. 3 A) SEM of G4 PAMAM templated TiO_2 formed in water, scale bar 1.67 μm. B) SEM of G4 PAMAM templated GeO_2 formed in water using TEOG as germanium alkoxide precursor, scale bar 667 nm. C) SEM of G4 PAMAM templated TiO_2 formed in phosphate buffer (100 mM, pH 7.5), scale bar 1.67 μm. D) SEM of G4 PAMAM templated GeO_2 formed in phosphate buffer (100 mM, pH 7.5) using TEOG as germanium alkoxide precursor, scale bar 3.75 μm.

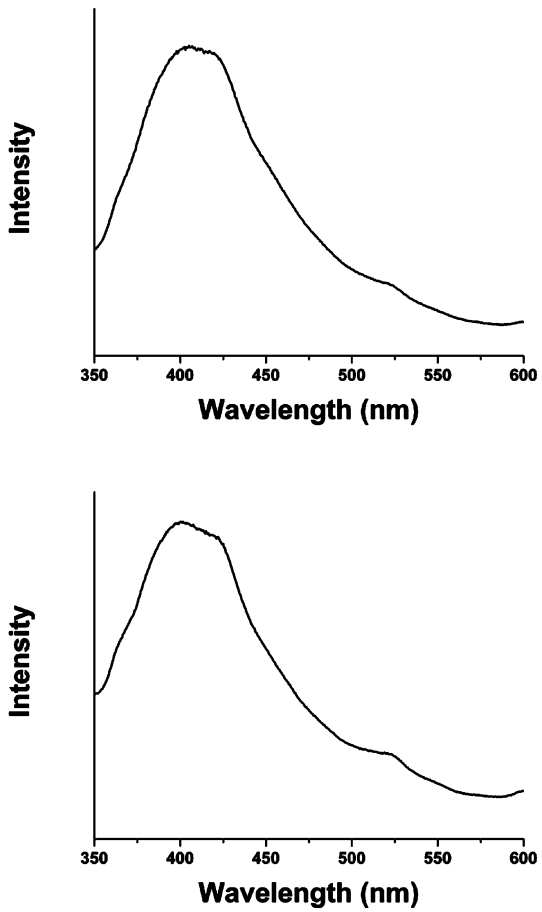

Fig. 4 Top: Photoluminescence spectrum for G4 PAMAM templated germanium dioxide in phosphate buffer (100 mM, pH 7.5) using TEOG as the germanium alkoxide precursor. Bottom: Photoluminescence spectrum for G4 PAMAM templated germanium dioxide in water using TEOG as the germanium alkoxide precursor.

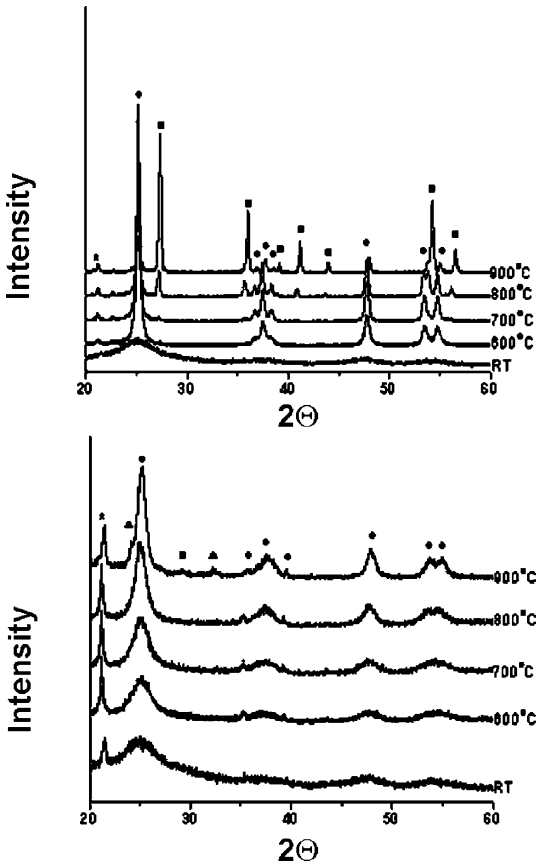

Fig. 5 Top: Variable temperature XRD of G4 PAMAM templated TiO_2 in water. Bottom: Variable temperature XRD of G4 PAMAM templated TiO_2 in phosphate buffer, 100 mM, pH 7.5 (● anatase, ■ rutile, and ▲ titanium phosphate, * silica plate).

titanium phosphate phase ($Ti_4P_6O_{23}$) began to form at approximately 700 °C. Previously this phase has been formed at 770 °C in deammination reactions of $NH_4Ti_2P_3O_{12}$ and the biomimetic synthesis of TiO_2 using the R5 peptide.[20,68,69] Here, liberated NH_4^+ from the degrading dendrimer or the NH_4^+ counterion from the precursor could mediate the reaction, forming $Ti_4P_6O_{23}$. Further, the onset of the anatase to rutile phase transition temperature is delayed by 200 °C relative to aqueous preparations, appearing at approximately 900 °C. Previously, it has been shown that phosphate ions incorporated into the titanium dioxide lattice retard the transition from anatase to rutile.[70] These experimental results are consistent with this mechanism of transition.

XRD analysis of the GeO_2 nanoparticles templated in either water or phosphate buffer revealed crystalline α-GeO_2 (Fig. 6A, B and ESI†). Additionally, selected area diffraction patterns of GeO_2 nanoparticles formed in the presence and absence of phosphate buffer indicated a crystalline structure (Fig. 7). When G4 PAMAM templated GeO_2 in either phosphate buffer or water was heated as high as 900 °C, no phase transitions were observed (ESI†). Furthermore, a germanium phosphate species was not observed, consistent with the IR analysis. Previously, crystalline α-GeO_2 has been formed in reverse micelle synthesis using the organic solvents heptane or octane, as well as high temperature synthesis procedures.[56,65,71]

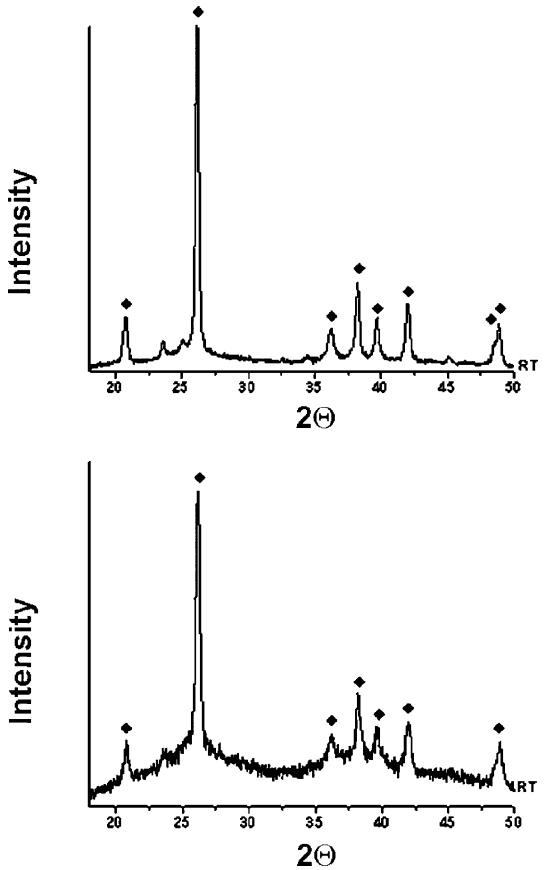

Fig. 6 Top: XRD of G4 PAMAM templated GeO_2 in water using TEOG as the germanium alkoxide precursor. Bottom: XRD of G4 PAMAM templated GeO_2 in phosphate buffer, 100 mM, pH 7.5, using TEOG as the germanium alkoxide precursor (◆ α-phase).

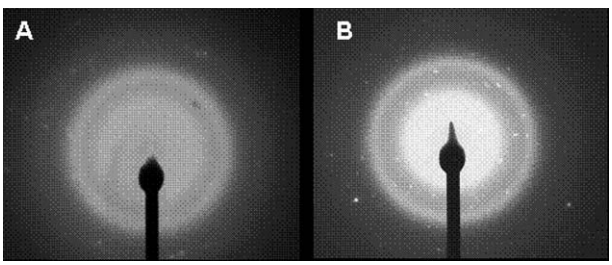

Fig. 7 A) Selected area diffraction pattern of GeO_2 nanoparticles synthesized in phosphate buffer using TEOG as the precursor (100 mM, pH 7.5). B) Selected area diffraction pattern of GeO_2 nanoparticles synthesized in water using TEOG as the precursor.

In the dendrimer mediated synthesis of TiO_2 and GeO_2, the substrates are hydrolyzed during the reaction. In the case of TBALDH, the amine rich dendrimer template likely acts as a general acid/base catalyst by protonating the lactate ligand, driving hydrolysis. Based on the pK_a of the dendritic primary amine groups,[72,73] a similar mechanism could occur with the germanium alkoxide precursors, where the alkoxide group is protonated by the dendrimer template, resulting in hydrolysis. Previously, nucleophilic mechanisms have been implicated in hydrolysis reactions involving biomimetic templates in aqueous

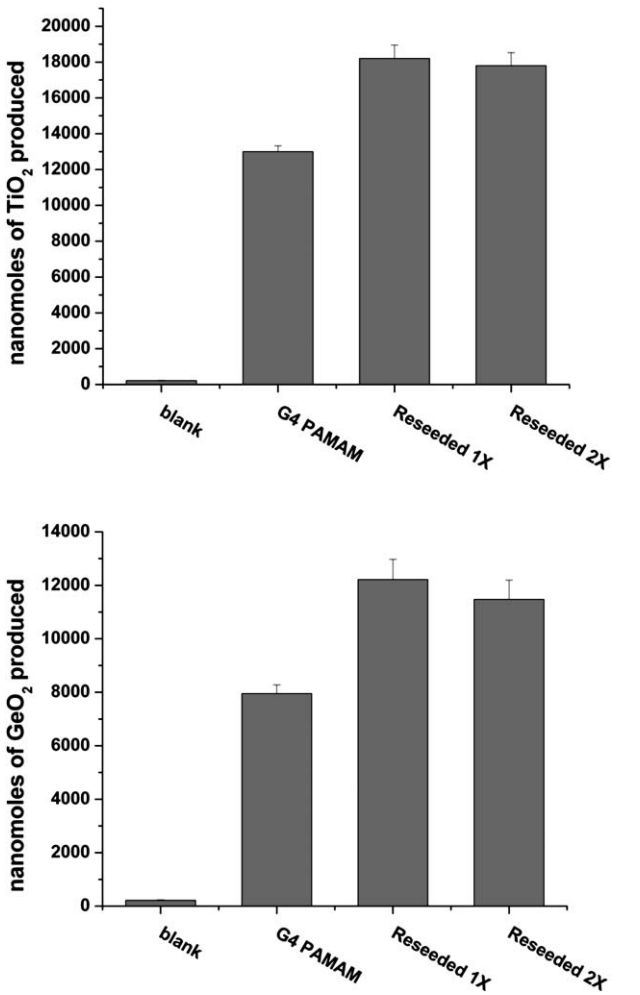

Fig. 8 Reseeding experiment for (top) TiO_2 and (bottom) GeO_2 (TEOG was used as the germanium alkoxide precursor).

solutions.[11,74–80] Further, the positively charged dendrimer template likely serves as a nucleation center by electrostatically interacting with the hydrolyzed precursor or the nascent metal oxide species. This interaction results in the encapsulation of the dendrimer template by the condensing metal oxide.[34] The particles continue to ripen and aggregate in solution, until a critical size is reached and flocculation occurs.

Previously, it has been shown that particle size and aggregation is influenced by the presence of cations provided by the simple salts of buffers.[33,47] These cations stabilize the charge of the growing negative particles, reducing the electrostatic repulsions, allowing smaller particles to aggregate in solution. While there are no cations present from phosphate buffer in the "water" reactions, the reaction conditions offer alternate sources of indigenous cations. In the case of TiO_2, the NH_4^+ cation associated with precursor may act as a stabilizing agent by shielding the slight negative charge on the growing nanosphere. Further, the positive charge of the dendrimer itself can also play a role in stabilizing the growing aggregate.

To examine the availability of the cationic dendrimer in the ripening phase of aggregate formation, a series of reseeding experiments were performed. Nanoparticles of TiO_2 produced from the G4 PAMAM template were collected by centrifugation,

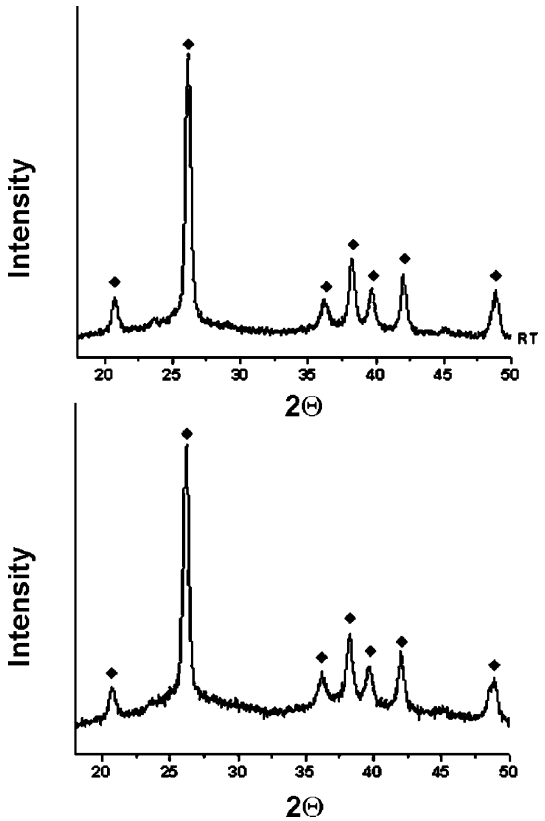

Fig. 9 Top: XRD of G4 PAMAM templated GeO_2 in water using TMOG as the precursor. Bottom: XRD of G4 PAMAM templated GeO_2 in phosphate buffer, 100 mM, pH 7.5, using TMOG as the precursor (◆ α-phase).

extensively washed, and then the appropriate precursor was introduced into solutions of the nanoparticles. These experiments reveal that when additional precursor is introduced into exhaustively washed TiO_2 nanoparticles, additional TiO_2 forms (Fig. 8A). These results support the idea that dendrimers are located on the surface of the nanoparticles, stabilizing the negative charge of the forming metal oxide. In the case of GeO_2 synthesis, there are no ions associated with the precursor, yet nanoparticles still formed in water. Reseeding experiments revealed that when the germanium alkoxide precursor is introduced into isolated and exhaustively washed GeO_2 particles, additional GeO_2 forms, indicating that the dendrimers not only act as the templating agent, but also are on the surface of the particles, shielding the negative charge of the growing particles (Fig. 8B). Therefore, even in solutions where there are no indigenous cations from either the precursor or buffer system, the positively charged dendritic template can act as a stabilizing agent.

To our knowledge, this is the first report of crystalline GeO_2 synthesized under mild, aqueous conditions. The rapid rate of hydrolysis may be contributing to the formation of crystalline GeO_2. Light scattering profiles of the G4 PAMAM mediated metal oxide synthesis reactions indicate that there is a rapid nucleation followed by nanoparticle growth, then flocculation from solution (ESI†). This conclusion is evinced by the sharp increase in scattering due to the rapid formation of particles. The light scattering profiles also indicate that GeO_2 formation occurs almost three times as quickly as TiO_2 formation. Furthermore, when the steric bulk of the precursor is varied, the crystallinity of the material is affected. Use of either TMOG or TEOG, which exhibit a rapid rate of hydrolysis,[81] as precursor results in crystalline GeO_2 (Fig. 9A and B). In contrast, when TIPG, which has a slower rate of hydrolysis,[81] was used as a substrate, amorphous GeO_2 was obtained (ESI†). The rapid rate of non-bulky alkoxide hydrolysis may lead to an immediately high concentration of the hydroxy precursor, resulting in a templating effect that mediates the formation of crystalline materials. Additionally, if any hydrolyzed precursors are present in the reaction mixture, then only amorphous GeO_2 spheres are formed, emphasizing the importance of precursor purity in obtaining crystalline material. This suggests that previously reported amorphous GeO_2 obtained by reaction of TMOG or TEOG precursors and polymer mediators may be the results of alternative condensation pathways.[31]

Conclusions

Biomimetic synthesis is an attractive alternative route to many abiological materials that avoids harsh chemicals, temperatures, and pressures. The general acid/base dendrimer mediated SiO_2 reaction has been expanded to include alternative substrates. Herein, we have shown that dendrimers are effective biomimetic templates for not only silica formation, but also GeO_2 and TiO_2 nanoparticle synthesis. XRD analysis of dendrimer templated TiO_2 nanoparticles revealed that the presence of phosphate buffer retarded the phase transition from anatase to rutile, similar to previously synthesized biogenic TiO_2.[20] Additionally, careful control over the purity of the germanium alkoxide precursor allows for the preparation of crystalline GeO_2 under ambient, aqueous conditions.

Acknowledgements

The authors thank the National Science Foundation (CMS-0508404 and CHE-0196540) for support of this work.

References

1 *Transition Metal Oxides: Structure, Properties, and Synthesis of Ceramic Oxides*; 2nd edn, ed. C. N. R. Rao and B. Raveau, Wiley, New York, 1998.
2 C. C. Koch, *Nanostructured Materials*, William Andrew, Norwich, 2002.
3 J. M. Slocik, M. R. Knecht and D. W. Wright, *Encycl. Nanosci. Nanotechnol.*, 2004, **1**, 293–308.
4 J. S. Ishay, K. Riabinin, M. Kozhevnikov, H. von der Want and I. Stokroos, *Biomacromolecules*, 2003, **4**, 469–456.
5 I. Stokroos, L. Litinetsky, J. J. L. van der Want and J. S. Ishay, *Nature*, 2001, **411**, 654.
6 R. Blackmore, *Science*, 1975, **190**, 377–379.
7 P. M. Harrison, A. Treffry, T. H. Lilley and J. Inorg, *Biochemistry*, 1986, **27**, 287–293.
8 T. Douglas and V. T. Stark, *Inorg. Chem.*, 2000, **39**, 1828–1830.
9 M. Okuda, K. Iwahori, I. Yamashita and H. Yoshimura, *Biotechnol. Bioeng.*, 2003, **84**, 187–194.
10 H.-A. Hosein, D. R. Strongin, M. Allen and T. Douglas, *Langmuir*, 2004, **20**, 10283–10287.
11 J. N. Cha, K. Shimizu, Y. Zhou, S. C. Christiansen, B. F. Chemelka, G. D. Stucky and D. E. Morse, *Proc. Natl. Acad. Sci. U. S. A.*, 1999, **96**, 361–365.
12 Y. Zhou, K. Shimizu, J. N. Cha, G. D. Stucky and D. E. Morse, *Angew. Chem., Int. Ed.*, 1999, **38**, 779–782.
13 J. L. Sumerel, W. Yang, D. Kisailus, J. C. Weaver, J. H. Choi and D. E. Morse, *Chem. Mater.*, 2003, **12**, 4804–4809.

14 D. Kisailus, J. H. Choi, J. C. Weaver, W. Yang and D. E. Morse, *Adv. Mater.*, 2005, **17**, 314–318.
15 N. Kroger, S. Lorenz, E. Brunner and M. Sumper, *Science*, 2002, **298**, 584–586.
16 N. Kroger, R. Deutzmann, C. Bergsdorf and M. Sumper, *Proc. Natl. Acad. Sci. U. S. A.*, 2000, **97**, 14133–14138.
17 N. Kroger, R. Deutzmann and M. Sumper, *Science*, 1999, **286**, 1129–1132.
18 N. Kroger, R. Deutzmann and M. Sumper, *J. Biol. Chem.*, 2001, **276**, 26066–26070.
19 M. R. Knecht and D. W. Wright, *Chem. Commun.*, 2003, 3038–3039.
20 S. L. Sewell and D. W. Wright, *Chem. Mater.*, 2006, **18**, 3108–3113.
21 N. Kroger, M. B. Dickerson, G. Ahmad, Y. Cai, M. S. Haluska, K. H. Sandage, N. Poulsen and V. C. Sheppard, *Angew. Chem., Int. Ed.*, 2006, **45**, 7239–7243.
22 S. V. Patwardhan and S. J. Clarson, *J. Inorg. Organomet. Polym.*, 2003, **13**, 193–203.
23 S. V. Patwardhan and S. J. Clarson, *J. Inorg. Organomet. Polym.*, 2003, **13**, 49–53.
24 S. V. Patwardhan, N. Mukherjee and S. J. Clarson, *Silicon Chem.*, 2002, **1**, 47–55.
25 S. V. Patwardhan, N. Mukherjee and S. J. Clarson, *J. Inorg. Organomet. Polym.*, 2001, **11**, 193–198.
26 S. V. Patwardhan, N. Mukherjee and S. J. Clarson, *J. Inorg. Organomet. Polym.*, 2001, **11**, 117–121.
27 S. V. Patwardhan and S. J. Clarson, *Silicon Chem.*, 2002, **1**, 207–214.
28 M. M. Tomczak, D. D. Glawe, L. F. Drummy, C. G. Lawrence, M. O. Stone, C. C. Perry, D. J. Pochan, T. J. Deming and R. R. Naik, *J. Am. Chem. Soc.*, 2005, **127**, 12577–12582.
29 T. Coradin and P. J. Lopez, *ChemBioChem*, 2003, **4**, 251–259.
30 T. Coradin, O. Durupthy and J. Livage, *Langmuir*, 2002, **18**, 2331–2336.
31 S. V. Patwardhan and S. J. Clarson, *Polymer*, 2005, **46**, 4474–4479.
32 A. Bouchara, L. Rozes, G. J. Soler-Illia and C. Sanchez, *J. Sol–Gel Sci. Technol.*, 2003, **26**, 629–633.
33 X.-B. Yu, Z.-H. Wang, H.-M. Chen, W.-M. Wang, S.-P. Yang and F. Zhang, *Mater. Lett.*, 2004, **58**, 3285–3289.
34 M. R. Knecht and D. W. Wright, *Langmuir*, 2004, **20**, 4728–4732.
35 Y. Nakanishi and T. Imae, *J. Colloid Interface Sci.*, 2005, **285**, 158–162.
36 Y. Nakanishi and T. Imae, *J. Colloid Interface Sci.*, 2006, **197**, 122–129.
37 K. Demadis and E. Neofotistou, *Chem. Mater.*, 2007, **19**, 581–587.
38 M. Allen, D. Willits, M. Young and T. Douglas, *Inorg. Chem.*, 2003, **42**, 6300–6305.
39 C. E. Flynn, C. Mao, A. Hayhurst, J. L. Williams, G. Georgiou, B. Iverson and A. M. Belcher, *J. Mater. Chem.*, 2003, **13**, 2414–2421.
40 M. B. Dickerson, R. R. Naik, M. O. Stone, Y. Cai and K. H. Sandhage, *Chem. Commun.*, 2004, 1776-1777.
41 M. R. Hoffmann, S. T. Martin, W. Choi and D. W. Bahnemann, *Chem. Rev.*, 1995, **95**, 69–95.
42 A. Wold, *Chem. Mater.*, 1993, **5**, 280–283.
43 X. L. Xu, L. X. Zhu, T. P. Chen, S. Fung and S. M. Li, *Thin Solid Films*, 1996, **283**, 230–234.
44 A. Margaryan and W. M. Liu, *Opt. Eng.*, 1993, **32**, 1995–1996.
45 M. S. Abdel-Aziz, K. A. Idriss and H. Sedaira, *Analyst*, 1996, **121**, 1079–1084.
46 R. K. Iler, *The Chemistry of Silica*, Wiley, New York, 1979.
47 M. R. Knecht, S. L. Sewell and D. W. Wright, *Langmuir*, 2005, **21**, 2058–2061.
48 R. R. Naik, P. W. Whitlock, F. Rodriguez, L. L. Brott, D. D. Glawe, S. J. Clarson and M. O. Stone, *Chem. Commun.*, 2003, 238–239.
49 *Structure Determination of Organic Compounds*, ed. E. Pretsch, P. Buhlmann and C. Affolter, Springer, Berlin, 2000.
50 P. A. Conner and A. J. McQuillan, *Langmuir*, 1999, **15**, 2916–2921.
51 J. C. Yu, L. Zhang, Z. Zheng and J. Zhao, *Chem. Mater.*, 2003, **15**, 2280–2286.
52 C. Combes, C. Rey and M. Freche, *Colloids ans Surfaces B: Biointerfaces*, 1998, **11**, 15–27.
53 T.-T. M. Isabel and M. A. Anderson, *Langmuir*, 1990, **6**, 602–611.
54 Y. Kanno and J. Nishino, *J. of Mater. Sci. Lett.*, 1993, **12**, 110–112.
55 T. Kawai, Y. Usui and K.-N. Kijiro, *Colloids Surf., A: Eng. Asp.*, 1999, **149**, 39–47.
56 H. P. Wu, J. F. Liu, N. Y. Ge, L. Niu, Y. W. Zeng, Y. W. Wang, G. L. Lv, L. N. Wang, G. Q. Zhang and J. Z. Jiang, *Chem. Mater.*, 2006, **18**, 1817–1820.
57 P. Viswanathamurthi, N. Bhattarai, H. Y. Kim, M. S. Khil, D. R. Lee and E. K. Suh, *J. Chem. Phys.*, 2004, **121**, 441–445.
58 J. Shi, J. Chen, Z. Feng, T. Chen, Y. Lian, X. Wang and C. Li, *J. Phys. Chem. C*, 2007, **11**, 693–699.
59 M. Zacharias and P. M. Fauchet, *Appl. Phys. Lett.*, 1997, **71**, 380–382.
60 X. C. Wu, W. H. Song, B. Zhao, Y. P. Sun and J. J. Du, *Chem. Phys. Lett.*, 2001, **349**, 210–214.
61 M. Zacharias and P. M. Fauchet, *J. Non-Cryst. Solids*, 1998, **227–230**, 1058–1062.
62 A. Trukhin, M. Kink, Y. Maksimov, J. Jansons and R. Kink, *J. Non-Cryst. Solids*, 2006, **352**, 160–166.
63 A. S. Zyubin, A. M. Mebel and S. H. Lin, *J. Chem. Phys.*, 2006, **125**, 064701.
64 J. Li, X. L. Wu, Y. M. Yang, X. Yang and X. M. Bao, *Phys. Lett.*, 2003, **314**, 299–303.
65 K. P. Kalyanikutty, G. Gundiah, A. Govindaraj and C. N. R. Rao, *J. Nanosci. Nanotechnol.*, 2005, **5**, 421–424.
66 Z. Jiang, T. Xie, G. Z. Wang, X. Y. Yuan, C. H. Ye, W. P. Cai, G. W. Meng, G. H. Li and L. D. Zhang, *Mater. Lett.*, 2005, **59**, 416–419.
67 R. D. Shannon and J. A. Pask, *Am. Mineral.*, 1964, **49**, 1707–1717.
68 A. Ono, *J. Solid State Chem.*, 1985, **56**, 260–262.
69 S. Horiuchi and A. Ono, *J. Solid State Chem.*, 1986, **62**, 335–341.
70 J. Criado and C. Real, *J. Chem. Soc., Faraday Trans.*, 1983, **79**, 2765–2771.
71 V. Simanzhenkov, H. Wiggers and P. Roth, *J. Nanosci. Nanotechnol.*, 2005, **5**, 436–441.
72 D. Leisner and T. Imae, *J. Phys. Chem. B*, 2003, **107**, 13158–13167.
73 D. Leisner and T. Imae, *J. Phys. Chem. B*, 2004, **108**, 1798–1804.
74 K. M. Delak and N. Sahai, *J. Phys. Chem. B*, 2006, **110**, 17819–17829.
75 K. M. Delak and N. Sahai, *Chem. Mater.*, 2005, **17**, 3221–3227.
76 J. N. Cha, G. D. Stucky, D. E. Morse and T. J. Deming, *Nature*, 2000, **403**, 289–292.
77 K. M. Roth, Y. Zhou, W. Yang and D. E. Morse, *J. Am. Chem. Soc.*, 2004, **127**, 325–330.
78 J. C. Weaver and D. E. Morse, *Microsc. Res. Tech.*, 2003, **52**, 356–367.
79 D. Kisailus, M. Najarian, J. C. Weaver and D. E. Morse, *Adv. Mater.*, 2005, **17**, 1234–1239.
80 S. V. Patwardhan, R. Maheshwari, N. Mukherjee, K. L. Kiick and S. J. Clarson, *Biomacromolecules*, 2006, **7**, 491–497.
81 *Chemistry of Advanced Materials*, ed. L. V. Interrante and M. J. Hampden-Smith, Wiley-VCH, New York, 1998.